STRUCTURAL OPTIMIZATION OF A FORCE-TORQUE SENSOR THROUGH ITS INPUT-OUTPUT RELATIONSHIP

R. Bekhti[1], V. Duchaine,[1], P. Cardou[2]
[1]*Department of Automated Manufacturing Engineering, École de Technologie Supérieure, Montréal, QC, Canada, rachid.bekhti.1@ens.etsmtl.ca; vincent.duchaine@etsmtl.ca*
[2]*Department of Mechanical Engineering, Université Laval, Québec, QC, Canada, pcardou@gmc.ulaval.ca*

ABSTRACT

We present an advanced method for optimizing the compliant structure of force-torque sensors at the design stage. In order to optimize the shape of the structural part of these sensors, some researchers used finite element analysis on several component of the compliant body, while others proposed performance indices based on mechanism theory. Currently, few of existing methods allow effective way design of force sensors to measure forces at different scales. This work proposes a new approach which includes a symbolic wrench-displacement relationship and optimization of the design parameters with respect to a given performance index. Our method is center on the application requirements, thus, it can take into account the constraints such as: the measurement range, the maximum allowable compliance or the physical dimensions. Once external forces are applied, the compliant structure must have a preset behavior to measure the displacements of preselected points in the mechanism, and thus, input-output relationship allows to match forces and theirs corresponding displacements to achieve suited sensitivity. Then, the resulting performance index can be expresses symbolically, which eases their synthesis tasks. The optimization procedure, design, fabrication and experiments of 3-axis force sensor architecture are presented and discussed.

Keywords: Force-torque sensor; design process; structural optimization.

OPTIMISATION STRUCTURELLE DE CAPTEURS DE FORCE-COUPLE VIA SA RELATION ENTRÉE-SORTIE

RÉSUMÉ

Nous présentons un processus de conception avancé de capteurs de force multi-axes en se basant sur l'optimisation structurelle de la partie compliante de celui-ci. Afin d'atteindre une méthode de conception optimale de structures de ces capteurs, certains chercheurs utilisent l'analyse par éléments finis sur plusieurs géométries du corps compliant créé par conception assistée par ordinateur. Tandis que d'autres utilisent des indices de performance tirés de la théorie des mécanismes. Ce travail propose une nouvelle approche qui inclut une relation symbolique force-déplacement et l'optimisation des paramètres de conception par rapport à un indice de performance. Notre méthode est centrée sur les spécifications de l'application et donc elle prend en considération les contraintes telles que : le spectre de force souhaité, la compliance maximale ou encore les dimensions physiques. En réponse aux forces externes appliquées, la structure compliante doit avoir un comportement prédéfini, et donc, la relation symbolique force-déplacement permet de faire correspondre les forces avec leurs déplacements correspondants pour obtenir une sensibilité adaptée. Alors, l'indice qui en résulte peut être exprimée symboliquement, ce qui facilite les tâches de synthèse. La procédure d'optimisation, la conception, la fabrication et les expérimentations sur une architecture de capteur de force 3-axes sont présentés et discutés.

Mots-clés : Capteur de force-couple ; processus de conception ; optimisation structurelle.

1. INTRODUCTION

A tremendous effort has been made in the recent years by the robotics community in order to bring robots into the same environment as humans [1]. This future coexistence will allow more flexibility [2] on production lines but could also open the door to the introduction of robots in our daily lives [3, 4]. However, there are still many challenges before achieving a good synergy between humans and robots. Robots will need to be mechanically designed to be inherently safe for humans but they should also have the intelligence to interact efficiently in our unstructured environment. These two desired characteristics will require progress in the fields of design and control but these robots will also need to have better sensing capabilities.

Multi-axis force-torque sensors is one of the key components that has been around for a long time [5] that could allow robots to interact with their surrounding environment. A force-torque sensor is a device, which uses its compliant body to perceive applied wrench vector. The deflection caused by the applied wrench will induce measurable displacements at preselected locations on the core of the sensor, usually a strain. Thus, the measurable displacement variation is able to convert to electrical signals and can be detected in various ways, commonly a voltage variation using strain gauges and Wheatstone's bridge [6].

Indeed, most of the commercial force-toque sensors use strain gauges as a technological means for inferring the applied wrench [7]. As pointed out by Hirose and Yoneda [8], this way of measuring displacements is responsible for the low precision and noise sensitivity of commercially available force-torque sensor. To circumvent these problems, researchers have proposed to use different measurement techniques such as optical [9, 10] or capacitive [11] sensing to measure the resulting internal displacement of a force sensor. However in our opinion, changing only the measurement technique is not sufficient alone to circumvent the lack of precision of existing force sensors [8]. In order to improve the force measurement quality we need a better understanding of the relationship between an applied wrench and the very small displacement of the compliant part of the sensor. Such knowledge would be a particularly powerful optimization for the design level to conceive a force-torque sensor that would take into account the specifications from an application (force and displacement range) while maximizing the use of the measurement signals on the quality of the force estimation. Bicchi [12] has presented a very interesting analysis of what should be the optimal criterion in the design of multi-axis force sensor, but this work was more at the level of defining a given optimal architecture than mechanically optimizing a real compliant structure.

This paper present a new optimum design method that uses analytical tools in order to define what should be the optimal structure, taking into account constraints such as the force measurement range, the maximum compliance and the physical dimensions.

Sections 2 and 3 presents respectively the mathematical analysis of the problem and the optimization procedure. Section 4 presents an application of our method to the design of a multi-axis force sensor, while section 5 describes its experimental validation using the designed prototype.

2. MATHEMATICAL ANALYSIS

2.1. Wrench-displacement relationship

For the sake of effectiveness and to clarify the dependence between the wrench-displacement relationship and the structure shape/geometry of the sensor, here we proposed a specific cantilever beam loading case where the force f is applied at the end (see Fig. 1). In this paper, we assume that the material which constitutes the force-torque sensor is homogeneous and isotropic. We also assume that the beam possess elastic behavior. Thus, small deformations led to proportional relation between the variation of displacement

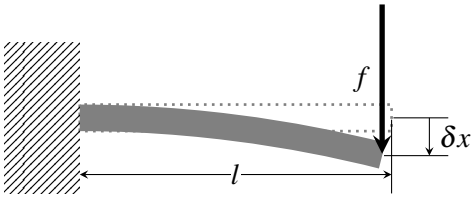

Figure 1. Cantilever beam diagram

δx and the force f, obeying so to the principle of classical static beam theory [13]. The relationship may be expressed by

$$f = k\delta x. \tag{1}$$

Using the definition of the Hooke's law, the stiffness of straight and uniform beam may be expressed as

$$k = \frac{3EI}{l^3}. \tag{2}$$

where E is the Young's modulus, $I = \frac{wh^3}{12}$ is the moment of inertia, f is the load applied over the beam, and l is the length of beam. From Eqs. (1) and (2), we highlight the importance of the cantilever beam geometry to define the relationship between the input (force) and the output (displacement) of the cantilever beam. In a case of mechanical structure for force-torque sensor, elaborating a model of stiffness is much more complex. Therefore, the dimensioning of the proper mechanical structure becomes more complex. In such a case, we cannot adopt a trial by error approach. In order to circumvent this heuristic approach, we used a generic model of stiffness which we will detail in the following subsection.

2.2. Elastostatic Model

We wish to obtain a relationship between the inputs and outputs of the force-torque sensor, the former being the applied wrench **w**, the latter being the displacements **x** of the suspended rigid mass. This is under the hypothesis that the material is perfectly elastic, and that the applied wrench varies at frequencies well below the lowest natural frequency of the structure, i.e., that the system can be assumed *quasistatic*.

Nowadays, the more popular approach to computing the wrench-displacement relationship is the finite element method. Although useful to model the elastostatic properties of complex architectures, this approach is numerically costly. For this reason, it does not seem the best suited for structural optimization, where the result quality depends on the number of designs solutions modeled and tested.

Here, we rather propose a symbolic model of the wrench-displacement relationship. The small displacements found in force-torque sensors and the fact that their compliant elements can generally be assimilated to Euler-Bernoulli beams make them good candidates for symbolic analysis. A symbolic model allows a deeper understanding of the relationships between the design parameters. In particular, it sheds light on the interplay between design parameters and cross-axis sensitivities. Finally, the computational cost of numerical methods like the FEM being generally greater, having a simple symbolical model speeds up computations, and allows the optimisation of the structure over numerous design parameters.

The elastostatic model we use is drawn from the *lumped* elastodynamic model proposed in [14]. "Lumped" refers to the assumption that the compliant elements act as massless ideal springs, whereas the other bodies are treated as rigid masses. Naturally, the elastostatic model is obtained by discarding the dynamic terms

from the elastodynamic model. This leaves us with the linear relationship between the applied wrench $\mathbf{w}$ and the mass displacements in space $\mathbf{x}$

$$\mathbf{w} = \mathbf{K}\mathbf{x}, \tag{3}$$

where $\mathbf{K} \in \mathbb{R}^{6\times 6}$ is the classical stiffness matrix.

The symbolic derivation of $\mathbf{K}$ is a long story, which revolves around the application of Castigliano's theorem to an expression of the potential energy based on screws. Because of space constraints, let us refer the reader to [14] for a complete account. Here, we simply state the resulting expression for the simpler case where there is only one rigid mass, its displacements being expressed in the fixed frame:

$$\mathbf{K} = \sum_{i=1}^{m} \left(\int_0^{l_i} \mathbf{S}_i(s_i)\mathbf{H}_i(s_i)\mathbf{S}_i(s_i)^T ds_i \right)^{-1}. \tag{4}$$

In this equation, l_i is the length of the i^{th} beam and s_i is a curvilinear coordinate along its neutral axis, as shown in Fig. 2. m is the number of beams acting in parallel to suspend the rigid mass. $\mathbf{S}_i$ is the twist-transfer matrix associated with screw $\mathbf{s}_i$, i.e., the matrix taking the wrench $\mathbf{u}_i$ applied on the i^{th} beam cross-section from frame $\mathscr{S}_i$ to frame $\mathscr{F}$. Symbolically, it is expressed as

$$\mathbf{S}_i = \begin{bmatrix} e^{\text{cpm}(\tau_i)} & \mathbf{0}_{3\times 3} \\ \text{cpm}(\sigma_i)e^{\text{cpm}(\tau_i)} & e^{\text{cpm}(\tau_i)} \end{bmatrix}, \text{ where } \mathbf{s}_i \equiv \begin{bmatrix} \tau_i \\ \sigma_i \end{bmatrix}, \tag{5}$$

$\tau_i \in \mathbb{R}^3$ is the array of the products of natural invariants of the rotation taking frame $\mathscr{F}$ onto $\mathscr{S}_i$, σ_i is the vector from O to S_i, and $\text{cpm}(\,\cdot\,)$ is the cross-product matrix[3]. Notice that $\mathbf{S}_i$ is a function of s_i through τ_i and σ_i, i.e., it varies according to the location where the cross-section of beam i is taken. Finally, $\mathbf{H}_i$ contains the properties of this cross-section, and is defined according to the strain energy formulas for beams:

$$\mathbf{H}_i(s_i) \equiv \text{diag}\left(\frac{1}{G_i J_i}, \frac{1}{E_i I_{Y,i}}, \frac{1}{E_i I_{Z,i}}, \frac{1}{E_i A_i}, \frac{\alpha_{Y,i}}{G_i A_i}, \frac{\alpha_{Z,i}}{G_i A_i} \right), \tag{6}$$

where E and G are the Young and the shear moduli, respectively; $I_{Y,i}$, $I_{Z,i}$ and J_i are the $Y_{\mathscr{S},i}$-axis moment of inertia, the $Z_{\mathscr{S},i}$-axis moment of inertia, and the torsional modulus of the beam cross section, respectively[4]; A_i is the area of the cross-section; and $\alpha_{Y,i}$ and $\alpha_{Z,i}$ are the shearing effect coefficients for the $Y_{\mathscr{S},i}$ and $Z_{\mathscr{S},i}$ directions, respectively. Notice that all these parameters could be functions of the curvilinear coordinate s_i, should the beam have a non-constant cross section.

3. OPTIMIZATION PROCEDURE

We do not satisfy ourselves with the improvement of the proposed force-torque sensor architecture from shear intuition, and propose a systematic optimization method for the selection of the design parameters from a given performance index. In addition, since the design parameters are always constrained by practical considerations, we included the displacement-sensor specifications, manufacturing tolerances, and other parameters as a set of equality and inequality constraints.

The optimization results depend on both the relevance of the mathematical model and efficiency of the optimization algorithm. Thus, the symbolic model we obtained from the Euler-Bernoulli beam theory allows the efficient computation of the stiffness matrix $\mathbf{K}$ from the decision variables. In turn, this stiffness matrix

[3] $\text{cpm}(\mathbf{a})$ is defined as $\partial(\mathbf{a}\times\mathbf{x})/\partial\mathbf{x}$, for any $\mathbf{a},\mathbf{x} \in \mathbb{R}^3$.

[4] $I_{Y,i}$, $I_{Z,i}$ and J are defined with respect to the centroid of the cross-section.

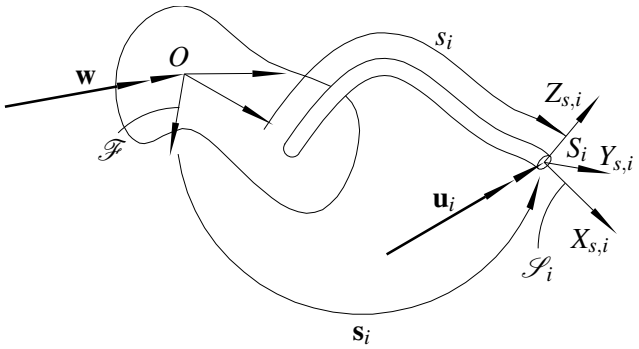

Figure 2. The suspended mass and its i^{th} compliant link

can be used to link a wrench applied on the suspended mass to the corresponding measurements picked up at the displacement sensors. The relationship is linear, and can thus be represented by the matrix $\mathbf{X} \in \mathbb{R}^{m\times 6}$, where m is the number of displacement sensors measuring the suspended mass motion. In fact, each column of the matrix represents the displacement of the tracked points of the suspended mass under a wrench applied in one of the principal directions. We thus refer to $\mathbf{X}$ as the "*characteristic displacement matrix*". Let us first detail how $\mathbf{X}$ is computed, and then explain how its condition number correctly represents the quality of the behavior of the force-torque sensor.

Let us consider that the structure have n degrees of freedom, where n is the number of generalized forces it is to measure, i.e., force and torque components. We also assume that the number of displacement sensors measuring the proof mass motion is m, which corresponds to the number of rows of $\mathbf{X}$. Let the i^{th} preselected point be equipped with a displacement sensor, and the j^{th} single axis force vector applied at a reference point of the suspended rigid mass. From Eq. (3), the six-dimension vector $\mathbf{x}$ gives the point displacement and orientation of the rigid mass in the fixed reference frame $\mathscr{F}$. We then establish a transformation matrix $\mathbf{T}_i$ between the fixed reference frame and the auxiliary reference frame $\mathscr{M}_i$ attached to the i^{th} displacement sensor. From these definitions and Eq. (3), the point displacement $\mathbf{x}_i$ seen by the corresponding displacement sensor under the action of wrench $\mathbf{w}$ becomes

$$\mathbf{x}_i = \mathbf{T}_i \mathbf{K}^{-1} \mathbf{w}, \tag{7}$$

where

$$\mathbf{T}_i = \begin{bmatrix} e^{\mathrm{cpm}(-\theta_i)}\mathrm{cpm}(\gamma_i) & e^{\mathrm{cpm}(-\theta_i)} \end{bmatrix}, \tag{8}$$

$\theta_i \in \mathbb{R}^3$ is the array of the products of natural invariants of the rotation taking frame $\mathscr{F}$ onto $\mathscr{M}_i$, and γ_i is the vector from the origin of $\mathscr{F}$ to that of $\mathscr{M}_i$. We then assume that each displacement sensor is uniaxial, with its sensitive direction given in frame $\mathscr{M}_i$ by unit vector $\mathbf{e}_i$. The displacement measurement from the i^{th} sensor due to the j^{th} principal wrench can thus be expressed as

$$x_{i,j} = \mathbf{e}_i^T \mathbf{T}_i \mathbf{K}^{-1} \mathbf{w}_j. \tag{9}$$

With $x_{i,j}$ being now available, the characteristic displacement matrix $\mathbf{X}$ is obtained as

$$\mathbf{X} = \mathbf{E}^T \mathbf{K}^{-1} \mathbf{W}, \tag{10}$$

where $\mathbf{E} \equiv [\mathbf{T}_1^T \mathbf{e}_1 \ \cdots \ \mathbf{T}_1^m \mathbf{e}_m]$ and $\mathbf{W} \equiv [\mathbf{w}_1 \ \cdots \ \mathbf{w}_n]$ is the matrix of principal wrenches to be applied on the suspended mass. These principal wrenches generally correspond to the extreme values of the forces and

moments that the force-torque sensor is to measure.

The condition number represent the relative gain in all sensitive directions in response to external loads. We want to make this gain as even as possible in all directions, which calls for minimizing the condition number. The objective function is therefore written as

$$\kappa = \|\mathbf{X}\|\|\mathbf{X}^{-1}\| = \frac{\sigma_{\max}(\mathbf{X})}{\sigma_{\min}(\mathbf{X})}, \tag{11}$$

where κ is the product of the norms. In order to evaluate the index between 0 and 1, we had rather choose the objective

$$1 - \frac{1}{\kappa}, \tag{12}$$

which is to be minimized. Notice that this index corresponds to the relative gain variation, as it may be expressed as

$$1 - \frac{1}{\kappa} = \frac{\sigma_{\max} - \sigma_{\min}}{\sigma_{\max}}. \tag{13}$$

We use a standard iterative algorithm to optimize the dimensions of the compliant structure forming the force-torque sensor. The analysis of the performance variations of an initial design allows iterative improvements. Having outlined the structural optimization procedure, let us apply it to the design of a force sensor in the following section.

4. OCTABEAMS FORCE SENSOR STRUCTURE

For an illustration of the core ideas of this paper, we developed a novel mechanical structure for a 3-axis force sensor called "*OctaBeams*", which is shown in Fig. 3. The adaptation of the theory presented in this paper to the 6-axis case should bear no difficulty. The mechanical structure of the sensor comprises of rigid central body, 8 square sectioned horizontal beams arranged symmetrically, and a rigid base. The choice of this structure architecture is not without purpose. In fact, the number and arrangement of beams guarantee the structure to resist twisting, thereby reducing sensitivity to moments about its axis of symmetry. In addition, the structure is stiff to forces applied orthogonal to its axis of symmetry, the displacement of the central rigid body is measured only in z direction using four displacement sensors symmetrically located under its suspended mass. To make things clearer, the measurement principle is clearly shown in Fig. 4.

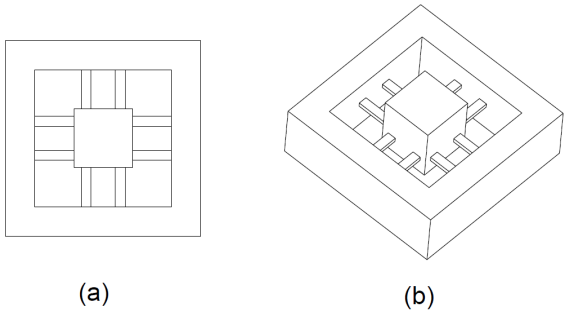

Figure 3. CAD of OctaBeams mechanical structure: (a) front view (b) isometric view.

After the selection of the 3-axis force sensor architecture, now we are ready to formulate the optimization problem specific to this sensor. Therefore, we defined the properties characterizing the force sensor such as

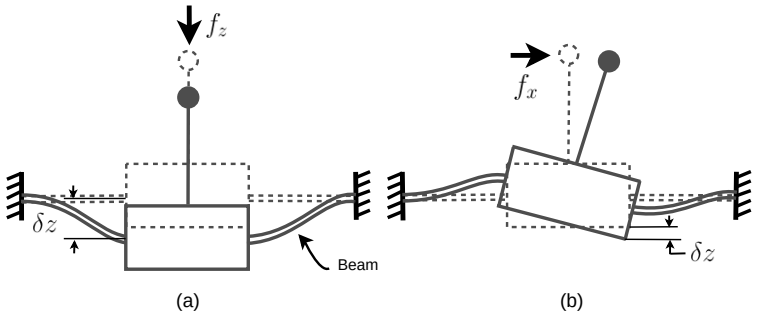

Figure 4. Scheme of the displacement measurement principle : (a) f_z load (b) fx load.

nominal applied forces, displacements ranges, material properties, and machining tolerances. The optimization problem can be expressed as follows: find the set of design parameters, h: thickness of the beam, w: width of the beam, l: length of the beam, such that they minimize the objective function given in Eq. (13), subject to :
- The force sensor fits in a square of 20 mm;
- The maximum applied forces are $f_x = 60$N, $f_y = 60$N and $f_z = 100$N;
- The displacements along the z direction under maximum applied forces range from 150um to 200um;
- The smallest milling tool diameter is 1/16";
- Aluminum 6061-T6 alloy or Delrin® is material composing the structure;
- Four displacement sensors are positioned at the edges of the square with 6.2mm side length, centered at the origin and fixed to the bottom face of the suspended rigid body.

In a follow-up experiment, we will study the role of the proposed index to achieve a better performance. For the sake of completeness and to show the versatility of the optimization procedure, we will develop rather two prototypes using different materials. However, only the aluminum version is used for the analysis and validation of the sensor performance. Indeed, the choice of aluminum is not casual. Once the sensor is built, it acts as a Faraday shield and immunizes the displacement sensors from the environment noise.

Considering the OctaBeams design parameters, the initial parameters are set as: $h = 1$ mm; $w = 1$ mm; and $l = 4.5$ mm. Using Aluminum as sensor material and the Matlab® optimization toolbox[5], the corresponding optimum design parameters are obtained. We find the following optimum dimensions: $h = 0.5$ mm, $w = 0.5$ mm, $l = 4.02$ mm. With the aim of improving the performance of the resulting sensor design, some tests in simulation and on a real structure should be conducted. Then, CAD model of the sensor structure has been developed according to the optimum dimensions. Figure. 5 shows the amplified displacements distributions of the OctaBeams structure under the forces f_x and f_z using *ProMechanica* FEM analysis. From this figure, it is clear that the behavior of the beams subjected to the force f_x or f_z is very close to what was expected in theory (see Fig. 4).

After the simulation, it is necessary to build a real prototype to validate the design method. Then, structures of OctaBeams force sensor has been machined in Aluminum material using a high precision CNC milling and some measures were performed. In addition, the displacements along the z direction under nominal applied forces were collected using a high precision force/displacement gauge. The results obtained from the CAD model and the real structure have been employed for the verification of the results and

[5]we resorted to constrained nonlinear optimization through the *fmincon* which uses an active-set algorithm.

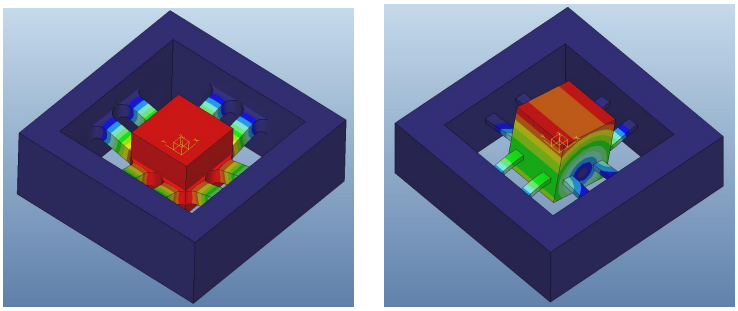

(a) (b)

Figure 5. Displacements resulting from the FEM analysis of OctaBeams aluminium structure: (a) f_z load (b), f_x load, displacements are amplified for the purposes of the visualization.

the comparison between the analytical, the numerical, and the real models, which are given in Tab. 1.

Table 1. Comparison between the displacements obtained by the symbolic model, the finite-element model, and the real structure.

Displacement in the z direction obtained from	fx	fy	fz	$1-\frac{1}{\kappa}$
The symbolic model (mm)	0.150	0.150	0.195	0.24
The finite − element model (mm)	0.145	0.144	0.207	0.29
Error between the symbolic and finite − element models (%)	3.33	4	5.79	/
The real structure (mm)	/	/	0.180	/

5. EXPERIMENTS AND DISCUSSION

5.1. Discussion

First, the experiments shows that optimum solution is found without violating the given constraints. Furthermore, the performance index reaches a sufficient value, which means that the relative gain sensitivity is roughly the same for all forces. Also, it can be observed from Tab. 1 that the maximum error between the symbolic and FEM models is 5.79%, which demonstrates the reliability of our symbolic stiffness matrix and that we can rely on it for the optimization. However, the difference between symbolic and FEM results is quite expected since both methods do not use the same principle of modeling. In the same way, differences of results between real prototype and those of FEM are not only due to the inaccuracies in the machining process, but also to the precision of the mesh and the numerical method used in FEM analysis. Nevertheless, differences between these three kinds of results remains negligible to question the validity of the symbolic analysis and the model of stiffness. In summary, despite the number of parameters and constraints, we consider our structural optimization procedure as reliable and relatively easy to implement.

5.2. Displacement sensors and conditioning electronics

In this subsection, we briefly describe the 3-axis force sensor displacement measurement principle and the integrated electronics. As regards to the small size of the sensor, our choice of displacement sensors technology was quite restrictive, thus, we decided to establish our displacement measurement on capacitive sensing. Several advantages are attributed to a capacitive measurement, such as: compactness in regards to other methods, non-contact devices, high-resolution measurement and ease of integration.

The displacement measurement principle we used is drawn from [15]. As shown in Fig. 6.a, two conductive plates are separated by a gap (air + silicon material), the top plate is attached to central rigid body. Whereas, the bottom plate is fixed to the base, knowing that the base is another part attached to the main structure. Since the area of plates remains constant, the capacitance is inversely proportional to the distance between the two plates. To keep the sensing only in z direction, lateral displacements are canceled by a specific design of the top plate such that the area of the parallel plate capacitors is constant up to a certain maximum lateral force.

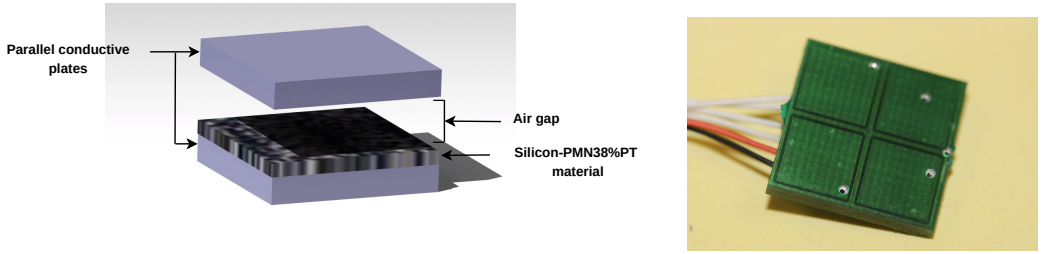

(a) (b)

Figure 6. (a) capacitive displacement measurement principle (b), photograph of the PCB.

The particular choice to use one layer of air and another of silicon material doped with nanoparticle of lead Magnesium Niobate-lead Titanate (PMN-PT) [6], as dielectric is relevant. Since the thickness of the sum of dielectric can vary without contact between plates, on one hand the stiffness of dielectric does not affect the displacements, on the other hand hysteresis effect is considerably reduced which increases the precision and repeatability of the sensor. Also, as the silicon is doped with PMN-PT, increases considerably the static dielectric constant. Therefore, this solution increases the signal amplitude for small applied forces. In other words, the resolution of the sensor is improved.

The capacitive to digital converter used for this prototype is an AD7147 made by Analog Devices. This ASIC was integrated to a PCB with 4 electrodes disposed on the top layer. These ones are configured in a way that the force along x, y and z axes can be theoretically measured without coupling. Indeed the force z is obtained by making the sum of the capacitance between all electrodes and the ground plane while x and y forces is given by a differential between two set of two electrodes. Figure. 6 shows a picture of the designed PCB. The measured capacitance values are send on a SPI bus to an external micro-controller.

5.3. Fabrication and calibration

In order to integrate the 3-axis force sensor presented in this paper, two force sensors were built using Delrin® and aluminum materials based on the optimization procedure described in section 4. The electronic board shown above were fixed, a cover and base parts were conceived and assembled to the main structures. A photograph of the 3-axis force sensor as constructed are shown in Fig. 7.

Once the 3 axis force sensor is manufactured, it must be calibrated. The calibration bench used in this paper is composed of : Mark® force gauge model M4-10, which has a measurement range of 50 N with a resolution of 0.02N, a 3-axis force sensor and SPI-RS232 card connected to a PC with Matlab® software installed. Furthermore, a calibration procedure is used to produce output signals. The calibration set-up and

[6] a ferroelectric ceramic with and incredibly high dielectric constant ($\varepsilon_r = 12500$)

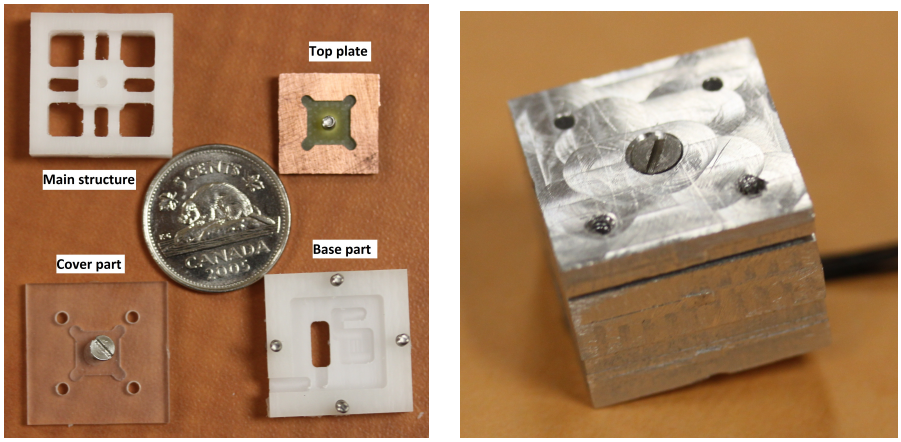

(a) (b)

Figure 7. 3-axis force sensor prototypes: (a) Delrin® assembling parts (b), assembled aluminum version.

the organization chart of the calibration system are shown in Fig. 8.

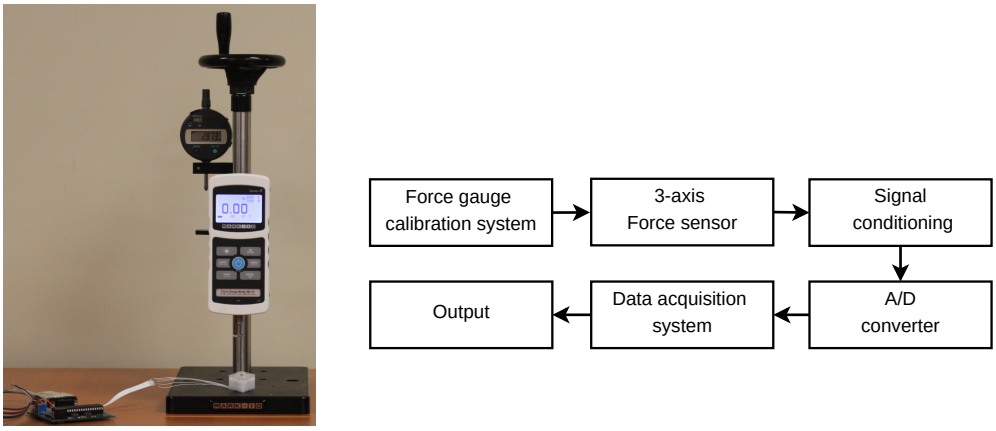

(a) (b)

Figure 8. The calibration system for 3-axis force sensor: (a) calibration set-up (b), schematic view.

The goal of the calibration procedure is to determine the relationship between the four capacitive output signals and the applied forces f_x, f_y and f_z. Using the collected output data, a fitting analysis is performed in order to calculate the optimal coefficients of the calibration law using a least-square method and polynomial of degree three. Given that the goal here is not to study the calibration laws, we simply show in Fig. 9 a comparison between the estimated and reference applied forces for some f_z force samples.

The targetted application for this 3 axis force sensor is an electromechanical active prosthesis socket for above-knee amputees that will be used to collect data about normal and shear stress. Since the amputation never occurs at the exact same place, conventional sockets are typically customized for each amputee. This uniqueness explains why there is almost no data available regarding the relationship between certain type of socket and certain type of fatigue injury occurring at the interface. This reconfigurable and instrumented socket will be used in a clinical environment to evaluate the stress resulting from different socket design.

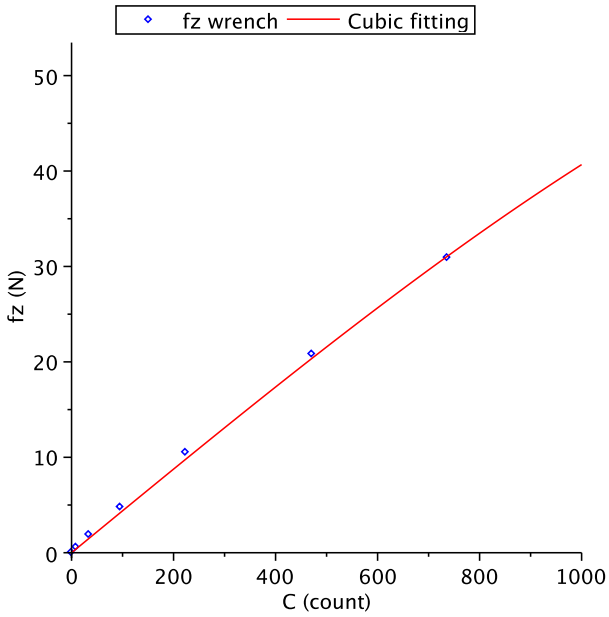

Figure 9. Graph of a f_z data fitting.

6. CONCLUSION

Proof of efficiency of the new structural optimization method for force-torque sensor was demonstrated in this paper. Using the symbolic relation of wrench-displacement, the aimed application specifications, a relevant and systematic method is formulated, which can be used even for designing accelerometers structures as well as compliant manipulators. Indeed, this is justified by the advantages attributed from this method. To make it more clear, the wrench-displacement relationship can be applied to different mechanical structures. Also, it is exhaustive, since fabrication limitations are defined before the optimization procedure, the force-torque sensor can be easily manufactured. Finally, it is generic, as the displacement sensor has non-contact, this method does not require information about the displacement sensor technology. We presented our work on 3-axis force sensor with some experimental tests in order to demonstrate the applicability of this method to a real design problem. Experiments show that the resulting satisfies all the design constraints. Nevertheless, further experiments and calibration needs to be performed to improve the performance of this sensor, such as its repeatability and its dynamic properties.

REFERENCES

1. De Santis, A., Siciliano, B., De Luca, A. and Bicchi, A. "An atlas of physical human–robot interaction." *Mechanism and Machine Theory*, Vol. 43, No. 3, pp. 253–270, 2008.
2. Brogårdh, T. "Present and future robot control, development of an industrial perspective." *Annual Reviews in Control*, Vol. 31, No. 1, pp. 69–79, 2007.
3. Kanda, T., Hirano, T., Eaton, D. and Ishiguro, H. "Interactive robots as social partners and peer tutors for children: A field trial." *Human-Computer Interaction*, Vol. 19, No. 1, pp. 61–84, 2004.
4. Mitsunaga, N., Miyashita, T., Ishiguro, H., Kogure, K. and Hagita, N. "Robovie-iv: A communication robot interacting with people daily in an office." In "Intelligent Robots and Systems, IEEE/RSJ International Conference," pp. 5066–5072. IEEE, 2006.
5. Whitney, D.T. "Historical perspective and state of the art in robot force control." In "Robotics and

Automation. IEEE International Conference," Vol. 2, pp. 262–268. IEEE, 1985.
6. Eslami, M. *Circuit Analysis Fundamentals*. 1 ed.. Agile Press, 2005.
7. Perry, D.M. "Multi-axis force and torque sensing." *Sensor Review*, Vol. 17, No. 2, pp. 117–120, 1997.
8. Hirose, S. and Yoneda, K. "Development of optical six-axial force sensor and its signal calibration considering nonlinear interference." In "Robotics and Automation, IEEE International Conference," pp. 46–53. IEEE, 1990.
9. Peirs, J., Clijnen, J., Reynaerts, D., Brussel, H.V., Herijgers, P., Corteville, B. and Boone, S. "A micro optical force sensor for force feedback during minimally invasive robotic surgery." *Sensors and Actuators: Physical*, Vol. 115, No. 2, pp. 447–455, 2004.
10. Takahashi, N., Tada, M., Ueda, J., Matsumoto, Y. and Ogasawara, T. "An optical 6-axis force sensor for brain function analysis using fmri." In "Sensors, Proceedings of IEEE," Vol. 1, pp. 253–258. IEEE, 2003.
11. Beyeler, F., Muntwyler, S. and Nelson, Bradley, J. "A six-axis mems force–torque sensor with micro-newton and nano-newtonmeter resolution." *Journal of Microelectromechanical Systems*, Vol. 18, No. 2, pp. 433–441, 2009.
12. Bicchi, A. "A criterion for optimal design of multi-axis force sensors." *Robotics and autonomous systems*, Vol. 10, No. 4, pp. 269–286, 1992.
13. Carrera, E., Giunta, G. and Petrolo, M. *Beam Structures: Classical and Advanced Theories*. 1 ed.. John Wiley & Sons, 2011.
14. Cardou, P., Pasini, D. and Angeles, J. "Lumped elastodynamic model for mems: Formulation and validation." *IEEE Journal of Microelectromechanical Systems*, Vol. 17, No. 4, pp. 948–961, 2008.
15. Baxter, L.K. *Capacitive Sensors: Design and Applications*. 1 ed.. IEEE Press Series on Electronics Technology, 1997.